International Journal of Progressive Sciences and Technologies (IJPSAT)
ISSN: 2509-0119.
© 2026 Scholar AI LLC.
https://ijpsat.org/

Vol. 58 No. 2 August 2026, pp. 1631-1642

Coastal Upwelling Transport at Cape Sainte-Marie, Southern Madagascar: Contribution of The CUTI Index

Lia Florin REASA[1], Jacques Chrysologue RATSIMAVO[2], Sahoby LALAOHARISOA[3], Jean Eugène RANDRIANANTENAINA[4], Adolphe RATIARISON[5]

[1,2,] Laboratoire Dynamique de l'Atmosphère, du Climat et des Océans (DyACO), University of Toliara, P.O. Box 185, Toliara, Madagascar.

[3,5] Laboratoire Dynamique de l'Atmosphère, du Climat et des Océans (DyACO), University of Antananarivo, P.O. Box 906, Antananarivo, Madagascar.

Corresponding author: Lia Florin REASA, reasa.florin@gmail.com

(cc) BY

Abstract: This study aims to characterize upwelling transport south of Madagascar around Cape Sainte-Marie (25°S-27°S, 42°E-46°E), while distinguishing the contribution of wind forcing from that of regional ocean circulation. An annual CROCO simulation forced by ERA5 is analyzed in four boxes representing the western upstream area, the coastal Core 2 cell, the Cape Sainte-Marie sector, and the export pathway toward the southern gyre. Two diagnostics are computed from simulated velocities: $CUTI_{south}$, which measures outward transport across the southern boundary, and $CUTI_{box}$, which summarizes the mean exchange balance across the four boundaries. The results are compared with the Bakun index.

Surface transport is positive in boxes B2, B3, and B4, with a maximum at Cape Sainte-Marie. The correlation with the Bakun index confirms a clear wind-driven component in the Core 2 cell. At the cape, the difference between $CUTI_{south}$ and $CUTI_{box}$ reveals compensation by lateral exchanges. In the export box, positive meridional transport and a negative mean balance highlight a connection with the southern gyre and dynamics that cannot be explained by local wind forcing alone. The box-based CUTI analysis complements the Bakun index by distinguishing meridional transport, lateral exchanges, and export toward the southern gyre. It therefore describes Core 2 as an open cell connected to Cape Sainte-Marie and the regional circulation.

Keywords: coastal transport; Coastal Upwelling Transport Index; ocean circulation; CROCO model; Bakun index; southern gyre.

1. INTRODUCTION

Southern Madagascar is a highly dynamic oceanic region where wind, bathymetry, and regional currents generate coastal upwelling of major ecological importance, supporting high productivity and fisheries [8], [10]. Coastal upwelling is generally associated with Ekman transport produced by winds parallel to the coast. Surface water is displaced offshore and replaced by deeper, colder, and often nutrient rich water. The Bakun index represents this wind-driven component of upwelling, but it does not account for pressure gradient effects, lateral transports, recirculation, or mesoscale dynamics [3], [7]. To better represent these contributions, Jacox et al. [1] proposed the Coastal Upwelling Transport Index (CUTI), which combines an Ekman component and a geostrophic component of transport.

South of Madagascar, Ramanantsoa et al. [2] identified two main upwelling cells: Core 1, located to the southeast and associated with the East Madagascar Current and upwelling favorable winds, and Core 2, located west of Cape Sainte-Marie, mainly forced by coastal winds but also influenced by exchanges with the Mozambique Channel. In the Core 1 sector, recent work [9] confirmed the existence of upwelling from ROMS simulated ocean velocities around Lake Anony, without quantifying the transport or distinguishing its components. For the Core 2 cell, although Ramanantsoa et al. [2] highlighted the importance of wind in upwelling variability, the contribution of lateral exchanges, recirculation, and mesoscale dynamics remains to be clarified, and this quantification has not yet been carried out.

The objective of this article is to use CUTI to characterize upwelling transport at Cape Sainte-Marie, corresponding to the Core 2 cell defined by Ramanantsoa et al. [2], from a transport diagnostic calculated using CROCO model outputs. Transport is analysed in four boxes covering the upstream area, the coastal cell, the cape sector, and the export zone toward the southern gyre. Comparison with the Bakun index makes it possible to distinguish the wind related part of the transport from the part related to lateral exchanges and regional dynamics. This study is based on the premise that Cape Sainte-Marie upwelling does not result only from wind forcing, but also from an open circulation connecting the coastal cell, the cape, and the southern gyre.

2. Methodology and CROCO numerical model

The method is based on a simple principle: when part of the surface water is exported horizontally, it is compensated by an upward motion from the subsurface. This mechanism corresponds to upwelling. The Bakun index describes only the wind-driven part of this export through Ekman transport. CUTI is calculated from CROCO simulated currents and can therefore account not only for wind effects, but also for lateral exchanges, recirculation, and regional dynamics. The comparison between Bakun and CUTI thus distinguishes the wind-driven contribution to transport from the contribution related to ocean circulation.

2.1. Simulation and variables used

The CROCO model [5], inherited from ROMS [4], solves the primitive equations under the hydrostatic and Boussinesq approximations on an Arakawa-C grid with sigma vertical coordinates and KPP turbulent closure [6]. The simulation covers southern Madagascar between 42°E-46°E and 27°S-25°S, with a horizontal grid of 145 × 82 points and 40 sigma vertical levels. It covers a 360 days numerical annual cycle forced by atmospheric conditions for 2010, with a time step dt = 20 s and daily output frequency. The extracted variables are sea surface temperature, surface salinity, horizontal velocity components u and v, and grid parameters. The u and v velocities are mainly used to calculate CUTI transports across the boundaries of the analysis boxes. Sea surface temperature and salinity are used to identify the upwelling signature.

2.2. Calculation boxes

The calculations are performed in four CUTI boxes with fixed coordinates. This subdivision separates the upstream area, the Core 2 cell, the Cape Sainte-Marie sector, and the export zone toward the southern gyre.

Table 1. Coordinates and role of the four CUTI boxes

Box	Longitude	Latitude	Role in the subdivision
B1 western upstream	43.0-44.0°E	26.8-25.8°S	Western upstream / signal maturation area
B2 coastal Core 2	44.0-45.0°E	26.6-25.4°S	Coastal Core 2 cell / main upwelling
B3 Cape Sainte-Marie	45.0-46.0°E	26.6-25.6°S	Cape Sainte-Marie sector / current acceleration
B4 export toward the southern gyre	44.0-46.0°E	27.0-26.6°S	Export toward the southern gyre

International Journal of Progressive Sciences and Technologies (IJPSAT)
ISSN: 2509-0119.
© 2026 Scholar AI LLC.
https://ijpsat.org/
Vol. 58 No. 2 August 2026, pp. 1631-1642

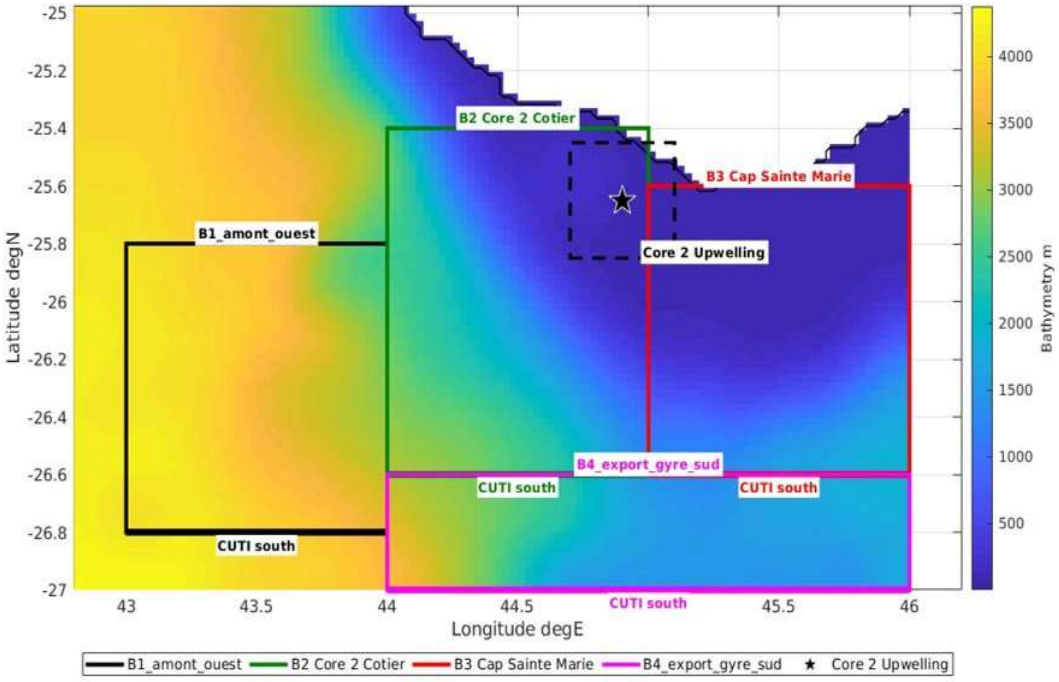


Figure 1. Location of the four CUTI boxes over the domain bathymetry (B1 western upstream; B2 coastal Core 2; B3 Cape Sainte-Marie; B4 export toward the southern gyre). The star marks the center of the Core 2 upwelling identified by Ramanantsoa et al. [2].

2.3. CUTI calculation

In the original formulation of Jacox et al. [1], CUTI is calculated as the sum of two contributions: an Ekman component, related to wind parallel to the coast, and a geostrophic component, related to sea level gradients. It is written as:

$$CUTI_{Jacox} = U_{Ek} + U_{Geo} \quad (1)$$

Where:

- U_{Ek} represents Ekman transport and U_{Geo} represents geostrophic transport.

This formulation complements the Bakun index, which represents only the wind-driven contribution to transport. In this study, the term CUTI refers to a surface transport diagnostic based on the principle of Jacox et al. [1], but calculated directly from CROCO simulated velocities at the boundaries of the analysis boxes, without separately reconstructing the Ekman and geostrophic components. This approach integrates the effect of wind and pressure gradients, as well as lateral exchanges, recirculation, and regional dynamics in the Core 2-Cape Sainte-Marie-southern gyre system. The calculation is based on the continuity equation, which expresses volume conservation in the surface layer:

$$\frac{\partial u}{\partial x} + \frac{\partial v}{\partial y} + \frac{\partial w}{\partial z} = 0 \quad (2)$$

The horizontal transports integrated over the surface layer [-H, 0] are defined as:

$$M_x = \int_{-H}^{0} u(z)dz \quad (3)$$

$$M_y = \int_{-H}^{0} v(z)dz \quad (4)$$

with H = 50 m. By integrating the continuity equation between the surface and depth -H, an estimate of vertical velocity at the base of the surface layer is obtained:

$$w(-H) = +\left(\frac{\partial Mx}{\partial x} + \frac{\partial My}{\partial y}\right) \quad (5)$$

International Journal of Progressive Sciences and Technologies (IJPSAT)
ISSN: 2509-0119.
© 2026 Scholar AI LLC.
https://ijpsat.org/
Vol. 58 No. 2 August 2026, pp. 1631-1642

This relation means that positive horizontal divergence of transport in the surface layer corresponds to upward motion at the base of that layer. It is the basis of the upwelling diagnostic used here. Within the analysis boxes, the CUTI associated with a boundary Γ is defined as the amount of water crossing the boundary outward from the box, integrated over the surface layer and then averaged along this boundary:

$$CUTI_{\Gamma} = \frac{1}{L\Gamma} \int_{\Gamma} \int_{-H}^{0} un(z)\, dz\, dl \qquad (6)$$

where L_Γ is the boundary length and u_n is the outward normal velocity component.

In this notation, Γ denotes one of the four boundaries of the analysis box (Γ_N, Γ_S, Γ_E or Γ_W), and dl is the line element along the boundary. The integral $\int_\Gamma$ dl therefore corresponds to a curvilinear integral calculated along the considered boundary. A positive value indicates outward transport from the box. For the four boundaries of each box, the adopted sign convention is as follows:

$$CUTI_{south} = -M_{y,south} \qquad (7a)$$

$$CUTI_{north} = +M_{y,north} \qquad (7b)$$

$$CUTI_{west} = -M_{x,west} \qquad (7c)$$

$$CUTI_{east} = +M_{x,east} \qquad (7d)$$

The main diagnostic is $CUTI_{south}$ because it measures outward transport toward the south in the surface layer. A positive $CUTI_{south}$ indicates surface export favorable to vertical compensation and upwelling. A second diagnostic, denoted $CUTI_{box}$, is defined to summarize the mean exchange balance through the four boundaries of each box:

$$CUTI_{box} = \frac{1}{4}(CUTIsouth + CUTInorth + CUTIwest + CUTIeast) \qquad (8)$$

$CUTI_{box}$ does not represent a total volume flux, but rather a mean value of exchanges across the four box boundaries, allowing the sign, relative intensity, and variability of exchanges among boxes to be compared. A value close to zero indicates that outward transports are broadly compensated by lateral inflows. A positive value reflects a tendency toward overall export according to the adopted sign convention, whereas a negative value indicates dominance of lateral inflows or a different dynamic compensation. This distinction is important for characterizing the open functioning of the Core 2-Cape Sainte-Marie-southern gyre system: $CUTI_{south}$ provides information on meridional export, whereas $CUTI_{box}$ provides information on the overall balance of exchanges across the four boundaries.

2.4. Bakun index calculation

The Bakun index is used here to represent the classical wind-driven component of coastal upwelling. In the historical formulation described by Bakun [3] and recalled by Jacox et al. [1], this index is based on Ekman theory: a wind stress parallel to the coast induces an Ekman transport perpendicular to the coast and directed offshore when the wind is favorable to upwelling. In this study, the surface wind-stress components are extracted from the CROCO atmospheric forcing and projected onto the alongshore direction, defined by the local angle θ, to obtain the alongshore wind stress τ_{along}.

$$I_{Bakun} = \frac{\tau alo}{(\rho_0 f)} \qquad (9)$$

where τ_{along} is the alongshore wind stress, ρ_0 is the reference seawater density, and f is the Coriolis parameter.

2.5. Statistical comparison between the Bakun and CUTI indices

The comparison between the Bakun index and CUTI evaluates the part of upwelling transport related to local wind forcing. The Bakun index mainly represents wind induced Ekman transport, whereas the CUTI diagnosed from CROCO also integrates the effects of simulated currents, lateral exchanges, recirculation, and regional dynamics. Correlations are calculated from daily time series. For each box, the Pearson correlation is estimated between the Bakun index and the two CUTI diagnostics:

$$r_{south} = corr(Bakun, CUTI_{south}) \qquad (10a)$$

$$r_{box} = corr(Bakun, CUTI_{box}) \qquad (10b)$$

International Journal of Progressive Sciences and Technologies (IJPSAT)
ISSN: 2509-0119.
© 2026 Scholar AI LLC.
https://ijpsat.org/
Vol. 58 No. 2 August 2026, pp. 1631-1642

The difference between the two correlations is defined as:

$$\Delta_r = r_{box} - r_{south} \quad (11)$$

A strong correlation between Bakun and $CUTI_{south}$ indicates that surface meridional export is strongly related to wind forcing. Conversely, a weak correlation shows that local wind does not fully explain the simulated transport. A large difference Δ_r between r_{box} and r_{south} means that the overall exchange balance across the four boundaries does not vary in the same way as the southern export. This difference indicates a possible influence of lateral transports, recirculation, and mesoscale dynamics.

2.6. Daily sampling and lag correlations

Correlations are also calculated with a temporal lag to identify any delay between wind forcing and the transport response diagnosed by CUTI:

$$r(\ell) = corr[Bakun(t), CUTI(t + \ell)] \quad (12)$$

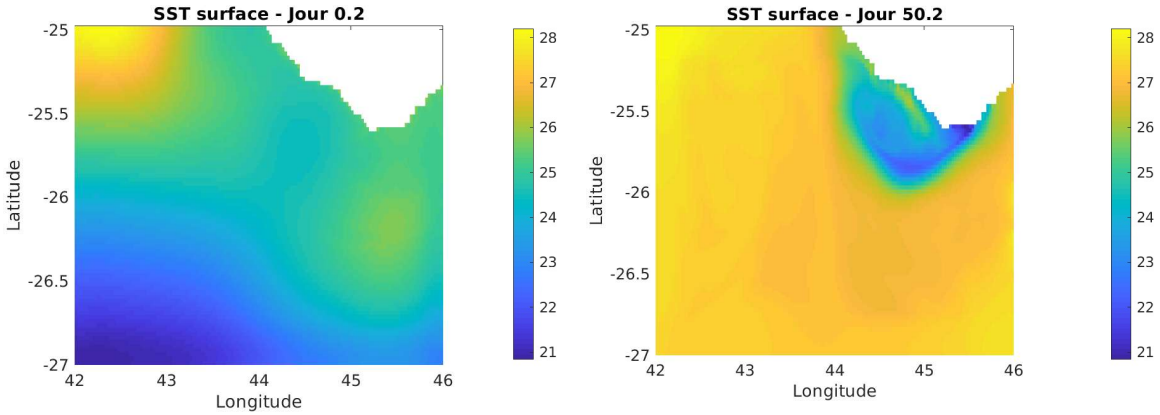
where ℓ is the lag expressed in days with daily sampling. In the convention used here, $\ell > 0$ means that the Bakun index precedes the CUTI response, whereas $\ell < 0$ means that the CUTI signal appears before the local wind signal. A maximum correlation close to zero days indicates a nearly simultaneous response to wind forcing. Significance tests account for time series autocorrelation through the use of an effective number of degrees of freedom N_{eff} [11]. Thus, a strong correlation between Bakun and CUTI indicates that a major part of the transport is related to wind forcing. Conversely, a weak correlation, or a maximum correlation shifted in time, suggests that upwelling transport also depends on other processes, such as lateral exchanges, recirculation, and mesoscale dynamics. In southern Madagascar, this approach distinguishes the response of the Core 2 cell, the role of the Cape Sainte-Marie sector, and export toward the southern gyre.

3. RESULTS

The results are presented in four steps: identification of the thermohaline upwelling signature, quantification of meridional export by $CUTI_{south}$, analysis of the lateral balance by $CUTI_{box}$, and comparison with the Bakun index to distinguish the wind-driven contribution from the dynamic contribution.

3.1. Upwelling signature

Sea surface temperature (SST) maps (Figure 2) show a clear sequence. On day 0, temperature is uniform and warm (≈ 27 °C). By day 50 (February), a cold tongue develops around Core 2 and the cape. The signal then detaches and spreads westward on days 100-150 (April-May). A broad cooling follows during austral winter, on days 200-250 (July-September).



International Journal of Progressive Sciences and Technologies (IJPSAT)
ISSN: 2509-0119.
© 2026 Scholar AI LLC.
https://ijpsat.org/
Vol. 58 No. 2 August 2026, pp. 1631-1642

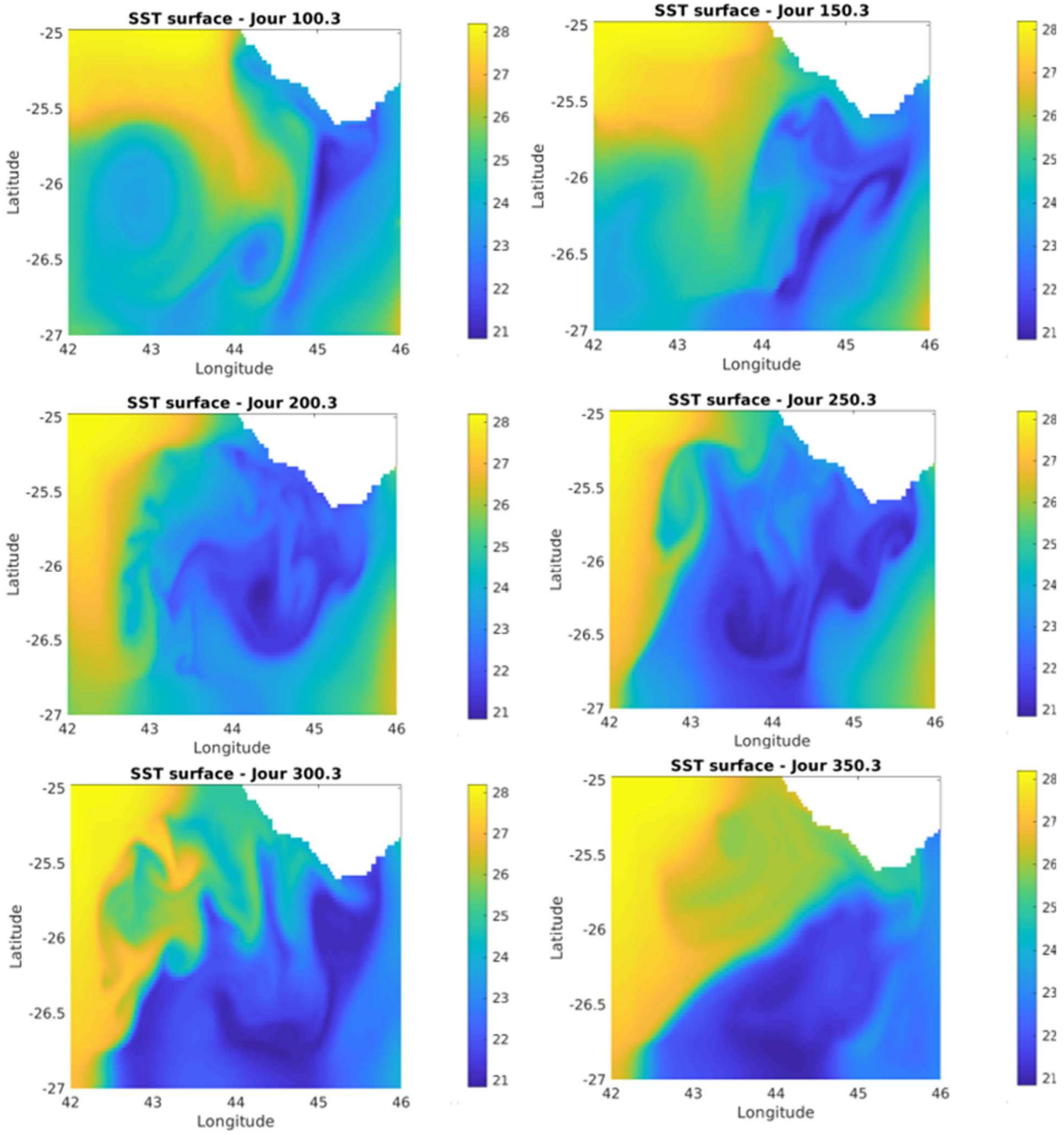


Figure 2. Sea surface temperature maps on days 0, 50, 100, 150, 200, 250, 300, and 350: birth of the cold tongue at the cape (day 50), westward detachment (days 100-150), and broad cooling during austral winter.

With the selected box subdivision, the mean SST of coastal Core 2 box B2 on day 50 is 25.66 °C, and the mean contrast between the other boxes (B1, B3, and B4) and B2 is 1.55 °C. During the cold phase J150-J280 (May-October), the maximum thermal contrast reaches 2.28 °C for B1-B2, 2.10 °C for B3-B2, and 2.91 °C for B4-B2, corresponding to a mean contrast of 2.43 °C. These contrasts confirm that B2 corresponds to the cold Core 2 cell.

Surface salinity maps (Figure 3) show a saltier anomaly appearing around Core 2 and the cape at the same time as the cold anomaly.

International Journal of Progressive Sciences and Technologies (IJPSAT)
ISSN: 2509-0119.
© 2026 Scholar AI LLC.
https://ijpsat.org/
Vol. 58 No. 2 August 2026, pp. 1631-1642

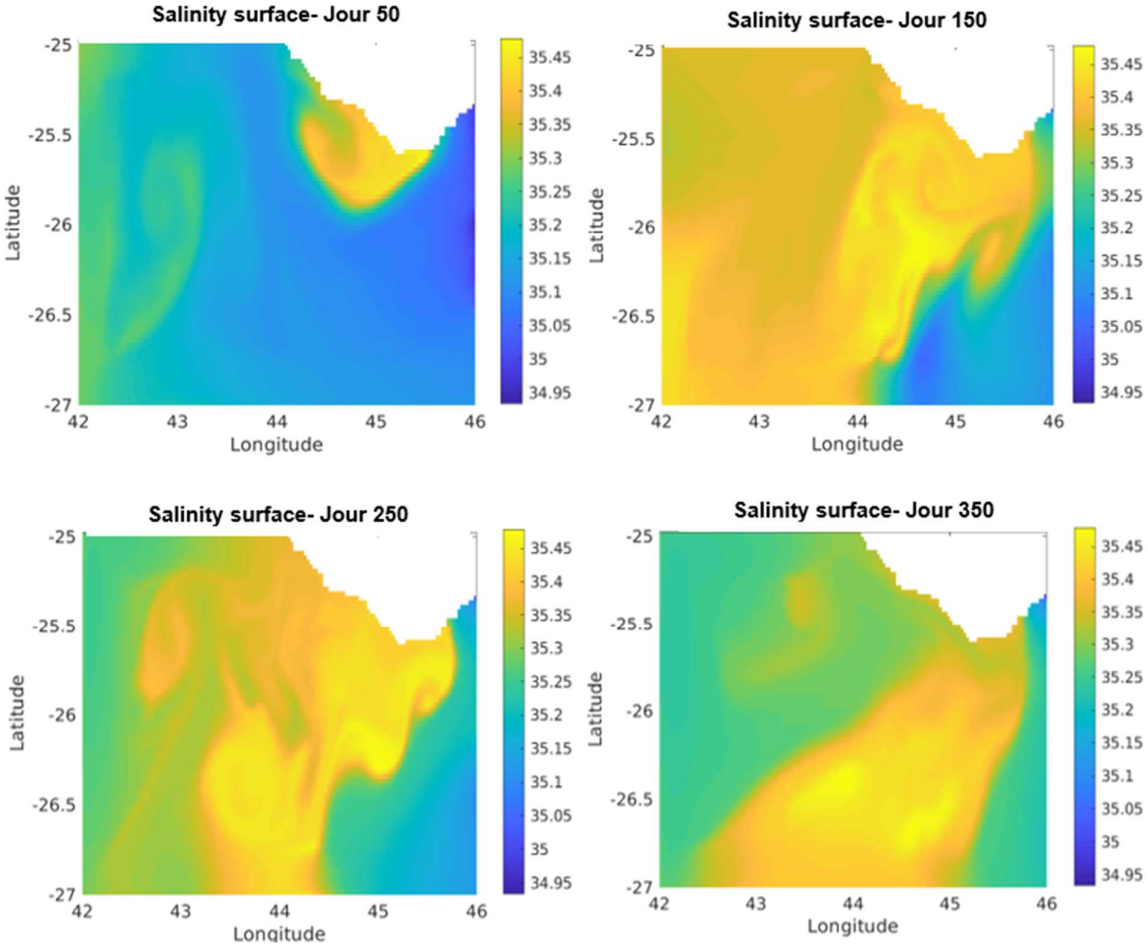


Figure 3. Surface salinity maps on days 50, 150, 250, and 350: salinization accompanies cooling, indicating water of subsurface origin.

Between the initial phase J0-J50 (January-February) and the final phase J300-J350 (October-December), salinity increases by 0.259 PSU in coastal Core 2 box B2, 0.284 PSU in Cape Sainte-Marie box B3, and 0.226 PSU in B4 export toward the southern gyre, corresponding to a mean increase of 0.256 PSU for B2-B3-B4. The simultaneity of surface cooling and salinization strongly suggests a contribution of colder and saltier subsurface waters to the upwelling signature. The thermohaline signature therefore confirms the existence of upwelling, which can then be quantified using transport indices.

3.2. Strengthening of $CUTI_{south}$ toward the cape sector

Mean $CUTI_{south}$ is positive in the four boxes: 0.58 ± 3.48 $m^2 \cdot s^{-1}$ in B1 western upstream, 4.11 ± 2.91 $m^2 \cdot s^{-1}$ in B2 coastal Core 2, 9.46 ± 3.46 $m^2 \cdot s^{-1}$ in B3 Cape Sainte-Marie, and 7.87 ± 2.54 $m^2 \cdot s^{-1}$ in B4 export toward the southern gyre (Figure 4). The positive value in B2 confirms surface export associated with the Core 2 cell. The maximum observed in B3 indicates that outward transport is particularly intense in the Cape Sainte-Marie sector. The high value in B4 also indicates that export toward the southern gyre remains an important component of the system.

International Journal of Progressive Sciences and Technologies (IJPSAT)
ISSN: 2509-0119.
© 2026 Scholar AI LLC.
https://ijpsat.org/
Vol. 58 No. 2 August 2026, pp. 1631-1642

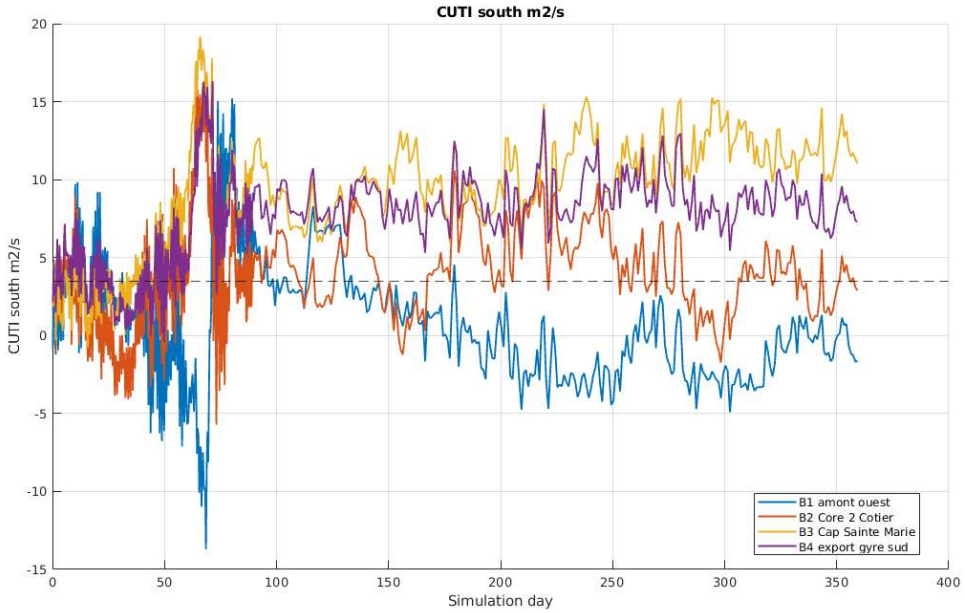


Figure 4. Daily evolution of $CUTI_{south}$ in the four analysis boxes.

3.3. Lateral balance in the cape sector and export zone

In coastal Core 2 box B2, the positive $CUTI_{south}$ (4.11 ± 2.91 $m^2 \cdot s^{-1}$) and moderately positive $CUTI_{box}$ (0.56 ± 0.35 $m^2 \cdot s^{-1}$; Figure 5) show that the cell is not isolated: it exchanges with neighboring boxes and with the cape sector.

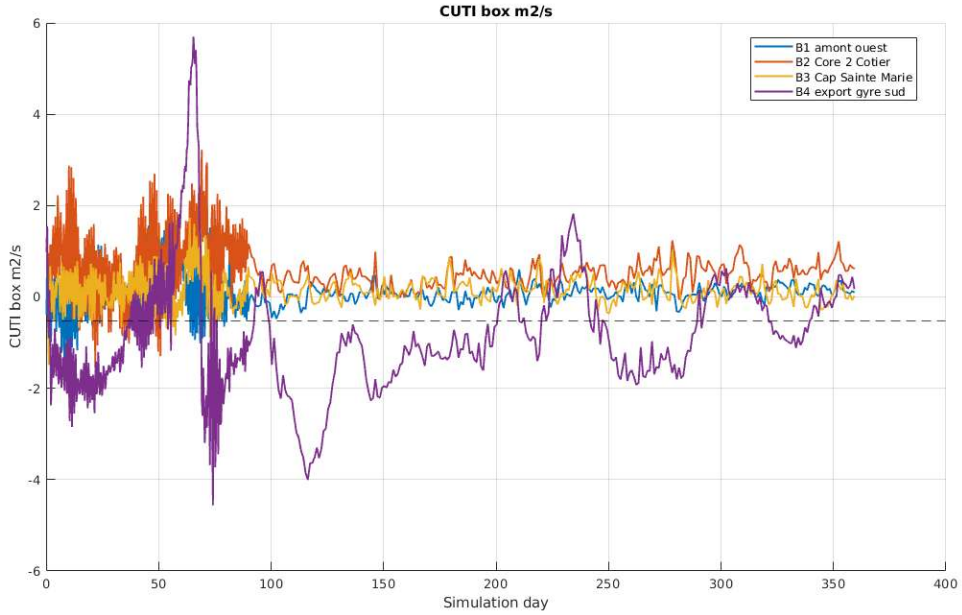


Figure 5. Daily evolution of $CUTI_{box}$ in the four analysis boxes.

International Journal of Progressive Sciences and Technologies (IJPSAT)
ISSN: 2509-0119.
© 2026 Scholar AI LLC.
https://ijpsat.org/
Vol. 58 No. 2 August 2026, pp. 1631-1642

In B3 Cape Sainte-Marie, $CUTI_{south}$ is higher (9.46 ± 3.46 $m^2 \cdot s^{-1}$), whereas $CUTI_{box}$ remains close to zero (0.16 ± 0.25 $m^2 \cdot s^{-1}$). The southern outflow is therefore compensated by lateral inflows. Finally, in B4 export toward the southern gyre, a positive $CUTI_{south}$ (7.87 ± 2.54 $m^2 \cdot s^{-1}$) associated with a negative $CUTI_{box}$ (-0.83 ± 1.25 $m^2 \cdot s^{-1}$) reflects a deficit balance, indicating a net export zone toward the southern gyre. Altogether, these results support the interpretation of Core 2 as an open cell connected to the cape and the southern gyre.

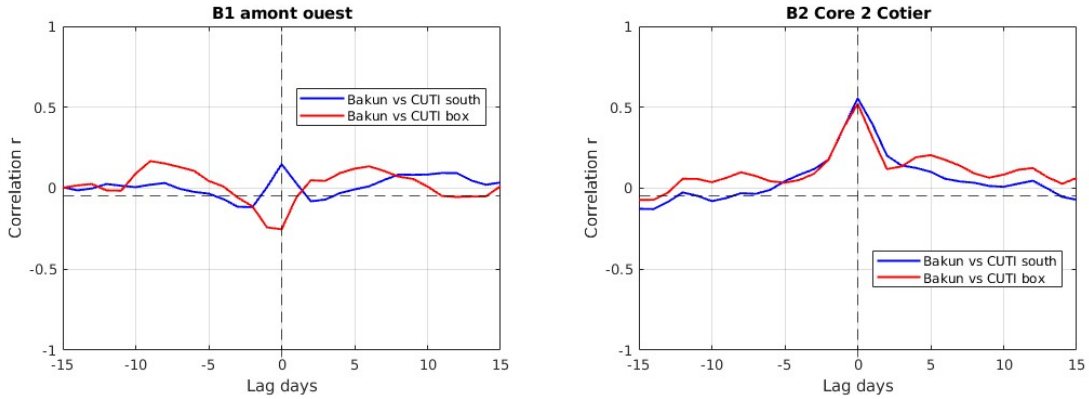
3.4. Separation of the wind-driven and dynamic components

The comparison with Bakun separates the wind-driven component from the dynamic component (Table 2, Figure 6). Correlations are calculated using daily time series (N = 360). In coastal Core 2 box B2, $CUTI_{south}$ is significantly correlated with Bakun ($r = 0.555$, $p < 0.001$). $CUTI_{box}$ is also significant there ($r = 0.521$, $p < 0.001$). The Core 2 cell therefore retains an identifiable wind-driven component, coherent between southern export and the box balance ($\Delta r \approx -0.03$). In B3 Cape Sainte-Marie, $CUTI_{box}$ is very strongly correlated with Bakun ($r = 0.724$, $p < 0.001$). By contrast, $CUTI_{south}$ shows only a weak but significant correlation ($r = 0.238$, $p < 0.05$). The difference $\Delta r = 0.486$ highlights a dissociation between the overall box balance and meridional transport at the cape. In B4 export toward the southern gyre, $CUTI_{south}$ is correlated with Bakun at zero lag ($r = 0.426$, $p < 0.001$). $CUTI_{box}$ is not significant at zero lag ($r = 0.147$) and reaches its maximum at a lag of -4 days ($r = 0.300$, $p < 0.01$). The box balance therefore also reflects lateral exchanges and gyre dynamics.

Table 2. Correlations between the Bakun index and CUTI diagnostics by box

Box	$CUTI_{box}$ / (lag 0)	$CUTI_{south}$ / (lag 0)	$CUTI_{box}$ peak	Interpretation
B1 western upstream	-0.253 / ($p < 0.01$)	0.149 / (n.s.)	-0.253 at 0 d	Box balance anti-correlated with wind
B2 coastal Core 2	0.521 / ($p < 0.001$)	0.555 / ($p < 0.001$)	0.521 at 0 d	Significant wind-transport coherence
B3 Cape Sainte-Marie	0.724 / ($p < 0.001$)	0.238 / ($p < 0.05$)	0.724 at 0 d	Strongly wind-related box balance; weakly wind-related southern boundary
B4 export toward the southern gyre	0.147 / (n.s.)	0.426 / ($p < 0.001$)	0.300 at -4 d	Meridional export, lateral exchanges, and -4 day lag

Note: n.s. = not significant ($p > 0.05$).



International Journal of Progressive Sciences and Technologies (IJPSAT)
ISSN: 2509-0119.
© 2026 Scholar AI LLC.
https://ijpsat.org/
Vol. 58 No. 2 August 2026, pp. 1631-1642

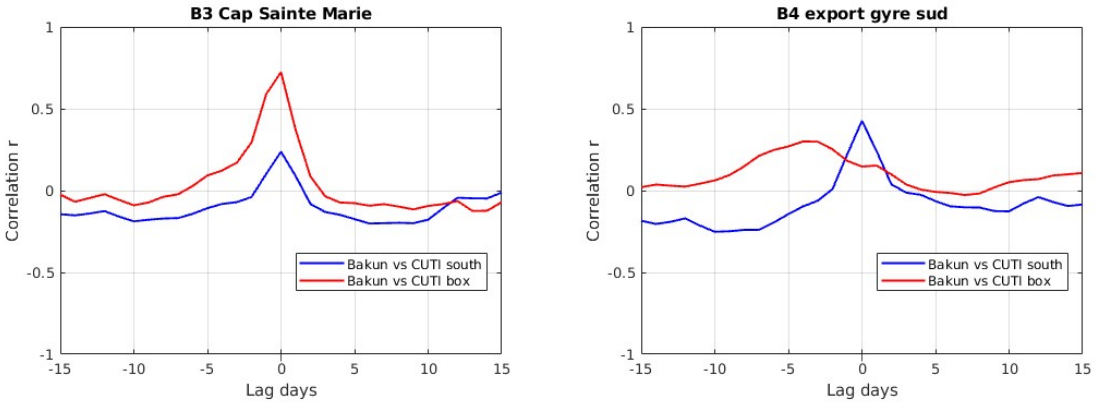


Figure 6. Lag correlations between the Bakun index and the $CUTI_{south}$ and $CUTI_{box}$ diagnostics in the four boxes.

4. DISCUSSION

The comparison between the Bakun index and CUTI shows the complementarity of the two approaches. The Bakun index represents the wind-driven component of transport, whereas CUTI diagnoses the transport simulated by CROCO from ocean currents. Their comparison thus distinguishes the part related to wind forcing from that associated with lateral exchanges, recirculation, and regional dynamics. The spatial structure of the indices, presented in Sections 3.2 and 3.3, shows a strengthening of $CUTI_{south}$ from the upstream area toward Cape Sainte-Marie. $CUTI_{box}$ is moderately positive in B2, close to equilibrium in B3, and negative in B4. This distribution reflects an open circulation connecting the Core 2 cell, the cape sector, and the export zone toward the southern gyre. This organization cannot be described by the Bakun index alone, because that index does not explicitly represent lateral transports, recirculation, or mesoscale processes.

The comparison between the two indices then identifies the dominant mechanisms in each sector. In the coastal Core 2 cell (B2), the strong correlations between Bakun and the two CUTI diagnostics, both $CUTI_{south}$ and $CUTI_{box}$, show that the transport is mainly related to wind forcing. At Cape Sainte-Marie (B3), the behavior differs: $CUTI_{box}$ remains strongly correlated with Bakun, whereas $CUTI_{south}$ shows only a weaker correlation. The difference between the two correlations ($\Delta r = 0.486$) indicates that meridional export does not respond only to local wind forcing and reflects the influence of other processes, including lateral exchanges, recirculation, and mesoscale dynamics. In the export zone toward the southern gyre (B4), the maximum correlation of $CUTI_{box}$ appears at a lag of -4 days. This lag indicates that the overall box balance also depends on gyre dynamics and not only on a direct response to wind.

The ability to identify a non-wind-driven part of the transport results from the methodological choice adopted in this study. Unlike the original CUTI formulation proposed by Jacox et al. [1], which reconstructs transport as the sum of an Ekman component and a geostrophic component, transport is diagnosed here directly from CROCO simulated currents at the boundaries of the analysis boxes. Jacox et al. [1] showed that this sum reproduces a large part of directly modelled transport, with about 80% of variance explained and a regression slope close to 1. The remaining 20% corresponds to the part of the transport that is not fully represented by this linear sum. This part may be associated with nonlinear processes, including advection, recirculation, and mesoscale transports. In the Cape Sainte-Marie region, the differences observed among the Bakun index, $CUTI_{south}$, and $CUTI_{box}$ indicate that the dynamic contribution cannot be neglected. The diagnostic adopted here therefore better integrates lateral exchanges, recirculation, and mesoscale processes in the characterization of upwelling transport.

These results complement the conclusions of Ramanantsoa et al. [2], who showed that the Core 2 cell is strongly related to upwelling-favorable winds, while also being influenced by exchanges with the Mozambique Channel. The correlation between Bakun and CUTI confirms the existence of a wind-driven component of the transport. However, the differentiated behavior of $CUTI_{south}$, $CUTI_{box}$, and B4 shows that local wind alone is not sufficient to explain the entire Core 2-Cape Sainte-Marie-southern gyre system.

5. CONCLUSION

The application of CUTI to coastal upwelling at Cape Sainte-Marie (Core 2) shows that the meridional transport diagnosed by $CUTI_{south}$ remains positive in the four analysis boxes. This transport is organized as an open circulation connecting the coastal cell, the Cape Sainte-Marie sector, and the export zone toward the southern gyre. Comparison with the Bakun index highlights contrasting behavior among sectors. In the coastal Core 2 cell (B2), the correlations indicate an identifiable wind-driven component of transport. At Cape Sainte-Marie (B3), the dissociation between $CUTI_{south}$ and $CUTI_{box}$ shows that meridional export does not depend only on local wind. In B4, positive $CUTI_{south}$ indicates surface export toward the southern gyre, whereas negative $CUTI_{box}$ reflects compensation by lateral exchanges in the overall box balance.

Thus, CUTI distinguishes the different components of upwelling transport more effectively than the Bakun index alone. It highlights both a wind-driven component, visible particularly in the Core 2 cell, and a dynamic component associated with lateral exchanges and export toward the southern gyre. The dynamic nature of this component and the climatological representativeness of these mechanisms will be examined, respectively, in a dedicated dynamic analysis and in a future multiyear study.

REFERENCES

[1] Jacox, M. G., Edwards, C. A., Hazen, E. L., Bograd, S. J. (2018). Coastal Upwelling Revisited: Ekman, Bakun, and Improved Upwelling Indices for the U.S. West Coast. Journal of Geophysical Research: Oceans, 123, 7332-7350.

[2] Ramanantsoa, J. D., Krug, M., Penven, P., Rouault, M., Gula, J. (2017). Coastal upwelling south of Madagascar: Temporal and spatial variability. Journal of Marine Systems, 178, 29-37.

[3] Bakun, A. (1973). Coastal Upwelling Indices, West Coast of North America, 1946–71. NOAA Technical Report NMFS SSRF-671.

[4] Shchepetkin, A. F., McWilliams, J. C. (2005). The Regional Oceanic Modeling System (ROMS): A split-explicit, free-surface, topography-following-coordinate oceanic model. Ocean Modelling, 9, 347-404.

[5] Debreu, L., Marchesiello, P., Penven, P., Cambon, G. (2012). Two-way nesting in split-explicit ocean models: Algorithms, implementation and validation. Ocean Modelling, 49-50, 1-21.

[6] Large, W. G., McWilliams, J. C., Doney, S. C. (1994). Oceanic vertical mixing: A review and a model with a nonlocal boundary layer parameterization. Reviews of Geophysics, 32, 363-403.

[7] Marchesiello, P., Estrade, P. (2010). Upwelling limitation by onshore geostrophic flow. Journal of Marine Research, 68, 37-62.

[8] Chavez, F. P., Messié, M. (2009). A comparison of eastern boundary upwelling ecosystems. Progress in Oceanography, 83, 80-96.

[9] Razafindramisa, H. L., Rasolozaka, N. M., Ratiarison, A. A. (2020). A Study of Ocean Velocity for Modelling the Upwelling of Seawater around the Anony Lake. American Journal of Fluid Dynamics, 10(1), 1-5.

[10] Longhurst, A. (2001). A major seasonal phytoplankton bloom in the Madagascar basin. Deep-Sea Research Part I: Oceanographic Research Papers, 48, 2413-2422.

[11] Bretherton, C. S., Widmann, M., Dymnikov, V. P., Wallace, J. M., Bladé, I. (1999). The effective number of spatial degrees of freedom of a time-varying field. Journal of Climate, 12, 1990-2009.